CCFE-PR(16)06

P. Jacquet et al

Maximization of ICRF Power by SOL Density Tailoring with Local Gas Injection

Maximization of ICRF Power by SOL Density Tailoring with Local Gas Injection

P. Jacquet[1], M. Goniche[2], V. Bobkov[3], E. Lerche[4,1], L. Colas[2], J. Hosea[5], S. Moriyama[6], R.I. Pinsker[7], S-J. Wang[8], S. Wukitch[9], X. Zhang[10], H. Bufferand[2], L. Guimarais[11], H. Faugel[3], G.R. Hanson[12], M. Kocan[13], I. Monakhov[1], J-M. Noterdaeme[3,14], V. Petrzilka[15], R.A. Pitts[13], A. Shaw[1], I. Stepanov[3,14], A.C.C. Sips[16], D. Van Eester[4], W. Zhang[3,14], the JET contributors[17], the ASDEX Upgrade team, the DIII-D team and the ITPA "Integrated Operation Scenarios" members and experts

[1]CCFE, Culham Science Centre, Abingdon, OX14 3DB, UK.
[2]CEA, IRFM, F-13108 Saint-Paul-Lez-Durance, France.
[3]Max-Planck-Institut für Plasmaphysik, Garching, Germany.
[4]LPP-ERM/KMS, EUROfusion Consortium Member - Trilateral Euregio Cluster, Brussels, Belgium
[5]Princeton Plasma Physics Laboratory, Princeton, NJ 08543, USA
[6]Japan Atomic Energy Agency, 801-1, Mukouyama, Naka, Ibaraki-ken 311-0193, Japan
[7]General Atomics, PO Box 85608, San Diego, CA 92186-5608, USA
[8]National Fusion Research Institute, Yuseong, Daejeon, 305-806, Republic of Korea
[9]MIT Plasma Science and Fusion Center, Cambridge, MA02139, USA
[10]Institute of Plasma Physics, Chinese Academy of Sciences, Hefei 230031, P. R. China
[11]Instituto de Plasmas e Fusão Nuclear, IST, Universidade de Lisboa, Portugal
[12]Oak Ridge National Laboratory, Oak Ridge, Teneessee, USA
[13]ITER Organization, Route de Vinon-sur-Verdon, CS 90 046, 13067 St. Paul Lez Durance Cedex, France
[14]Applied Physics Department, UGent, Gent, Belgium
[15]IPP.CR, Za Slovankou 3, 182 21 Praha 8, Czech Republic
[16]European Commission, B1049 Brussels, Belgium
[17]EUROfusion Consortium, JET, Culham Science Centre, Abingdon, OX14 3DB, UK

Maximization of ICRF Power by SOL Density Tailoring with Local Gas Injection

P. Jacquet[1], M. Goniche[2], V. Bobkov[3], E. Lerche[4,1], L. Colas[2], J. Hosea[5], S. Moriyama[6], R.I. Pinsker[7], S-J. Wang[8], S. Wukitch[9], X. Zhang[10], H. Bufferand[2], L. Guimarais[11], H. Faugel[3], G.R. Hanson[12], M. Kocan[13], I. Monakhov[1], J-M. Noterdaeme[3,14], V. Petrzilka[15], R.A. Pitts[13], A. Shaw[1], I. Stepanov[3,14], A.C.C. Sips[16], D. Van Eester[4], W. Zhang[3,14], the JET contributors[17,*], the ASDEX Upgrade team, the DIII-D team and the ITPA "Integrated Operation Scenarios" members and experts

[1]*CCFE, Culham Science Centre, Abingdon, OX14 3DB, UK.*

[2]*CEA, IRFM, F-13108 Saint-Paul-Lez-Durance, France.*

[3]*Max-Planck-Institut für Plasmaphysik, Garching, Germany.*

[4]*LPP-ERM/KMS, EUROfusion Consortium Member - Trilateral Euregio Cluster, Brussels, Belgium*

[5]*Princeton Plasma Physics Laboratory, Princeton, NJ 08543, USA*

[6]*Japan Atomic Energy Agency, 801-1, Mukouyama, Naka, Ibaraki-ken 311-0193, Japan*

[7]*General Atomics, PO Box 85608, San Diego, CA 92186-5608, USA*

[8]*National Fusion Research Institute, Yuseong, Daejeon, 305-806, Republic of Korea*

[9]*MIT Plasma Science and Fusion Center, Cambridge, MA02139, USA*

[10]*Institute of Plasma Physics, Chinese Academy of Sciences, Hefei 230031, P. R. China*

[11]*Instituto de Plasmas e Fusão Nuclear, IST, Universidade de Lisboa, Portugal*

[12]*Oak Ridge National Laboratory, Oak Ridge, Teneessee, USA*

[13]*ITER Organization, Route de Vinon-sur-Verdon, CS 90 046, 13067 St. Paul Lez Durance Cedex, France*

[14]*Applied Physics Department, UGent, Gent, Belgium*

[15]*IPP.CR, Za Slovankou 3, 182 21 Praha 8, Czech Republic*

[16]*European Commission, B1049 Brussels, Belgium*

[17]*EUROfusion Consortium, JET, Culham Science Centre, Abingdon, OX14 3DB, UK*

[*] See the Appendix of F. Romanelli et al., Proceedings of the 25th IAEA Fusion Energy Conference 2014, Saint Petersburg, Russia

Abstract. Experiments have been performed under the coordination of the International Tokamak Physics Activity (ITPA) on several tokamaks, including ASDEX Upgrade (AUG), JET and DIII-D, to characterize the increased ICRF antenna loading achieved by optimizing the position of gas injection relative to the RF antennas. On DIII-D, AUG and JET (with the ITER-Like Wall) a 50% increase in the antenna loading was observed when injecting deuterium in ELMy H-mode plasmas using mid-plane inlets close to the powered antennas instead of divertor injection and, with smaller improvement when using gas inlets located at the top of the machine. The gas injection rate required for such improvements (~0.7×10^{22}el/s in AUG, ~1.0×10^{22} el/s in JET) is compatible with the use of this technique to optimize ICRF heating during the development of plasma scenarios and no degradation of confinement was observed when using the mid-plane or top inlets compared with divertor valves. An increase in the scrape-off layer (SOL) density was measured when switching gas injection from divertor to outer mid-plane or top. On JET and DIII-D, the measured SOL density increase when using main chamber puffing is consistent with the antenna coupling resistance increase provided that the distance between the measurement lines of sight and the injection location is taken into account. Optimized gas injection was also found to be beneficial for reducing tungsten (W) sputtering at the AUG antenna limiters, and also to reduce slightly the W and nickel (Ni) content in JET plasmas. Modeling the specific effects of divertor/top/mid-plane injection on the outer mid-plane density was carried out using both the EDGE2D-EIRENE and EMC3-EIRENE plasma boundary code packages; simulations indeed indicate that outer mid-plane gas injection maximizes the density in the mid-plane close to the injection point with quantitative agreement with the SOL density measurements for EMC3-EIRENE. Field line tracing for ITER in the 15 MA Q_{DT}=10 reference scenario indicates that the planned gas injection system could be used to tailor the density in front the antennas, but more ITER SOL simulations are required to quantify the effect of gas injection on the SOL density in front of the antennas.

1. Introduction

Ion Cyclotron Range of Frequency (ICRF) wave heating of tokamak plasmas relies on the propagation and the absorption of the fast wave, which is evanescent until it reaches a plasma density which exceeds the cut-off value n_{e_CutOff} [1]. For the ICRF frequencies used to heat tokamak plasmas (~30-100 MHz) n_{e_CutOff} is in the 10^{18} m^{-3} range, which is typical of the Scrape-Off Layer (SOL) density. The ICRF power coupled to the plasma from the antenna can be expressed as: $P_{coupled} \sim V_{\max}^2 \, R_c / 2 Z_c^2$ (1)

where R_c is the antenna coupling resistance. The antenna is fed by transmission lines with characteristic impedance Z_c, and V_{max} is the anti-node voltage in the transmission line. In practice on many tokamaks, the ICRF power coupled to the plasma is limited by the increased risk of arcing in the transmission lines when V_{max} gets close to 35-45 kV (depending on the system). Fast wave power transfer increases when reducing the thickness of the evanescent layer d_{evan} (the far SOL region between the antenna and the plasma where $n_e<n_{e\_CutOff}$); wave propagation in the SOL is also affected by density gradients. It can be shown (see [2]) that the coupling resistance is expected to behave as:

$$Rc \propto \exp(-\alpha \ d_{evan}) \qquad (2)$$

where α is a tunneling factor that depends on the specific antenna geometry and on the density gradient at the cut-off position. This was verified experimentally, for example on AUG [3] and Tore-Supra [4]. In ITER there are significant uncertainties in the density profiles predicted in the SOL, which lead to large uncertainties in the predicted coupled power (between 10 MW and 20 MW per antenna limited by the installed generator power) using antenna simulation codes [5] and taking into account the various operating limits in the antenna system (e.g. maximum voltage at the straps and in the transmission lines, RF field at the 3-port junction, etc.) [6].

Some years ago, it was proposed to use local gas injection [7] as a tool to tailor the electron density in front of the ICRF antennas during the pulses and hence maximize or control the antenna coupling resistance. A similar technique is used to reduce the reflection coefficient of Lower Hybrid Current Drive antennas (see [8] and references therein). Experiments to assess the efficiency of this technique for ICRF heating have been performed under the coordination of the International Tokamak Physics Activity (ITPA) on ASDEX Upgrade (AUG) [9][10], JET [11][12], DIII-D [13][14], Tore-Supra and TEXTOR. This paper which concentrates on the recent experiments from AUG, JET and DIII-D, divertor devices of most relevance for ITER, summarizes these experiments, highlights the similarities or differences in the experimental results and describes the needs for modeling to assess the suitability of the location of ITER gas injection [15][16] for the purpose of ICRF coupling enhancement.

The paper is organized as follows: in Section 2 the machine parameters and experimental conditions are described for AUG, DIII-D, and JET. The JET experiments were performed with the ITER-Like Wall (ILW, tungsten divertor and beryllium wall). Section 3 describes

the experimentally observed effects of local gas injection on the SOL density, antenna coupling and other plasma parameters. In support of the experimental measurements, plasma boundary modelling using the EDGE2D-EIRENE code (for JET and AUG) and the EMC3-EIRENE package (for AUG) has been attempted and Section 4 describes the results. Concluding remarks and prospects for future work are offered in Section 5.

2. Experimental setups

The main parameters of the AUG, JET and DIII-D experiments from which results will be presented here are listed in Table 1. The geometry of the antennas, gas injection location and the lines of sight of the main diagnostics used in the experiments are shown in Figure 1, Figure 2 and Figure 3. Readers are invited to refer to these figures for the exact positions of antennas, gas inlets, diagnostics, etc., when following the description of the experiments. In all cases, divertor gas injection was toroidally distributed while Outer Mid-Plane (OMP) and top injection were toroidally localized. On JET, at each toroidal location, top gas injection was poloidally distributed (see Figure 2). We note that on JET the term GIM is used locally to denote "Gas Injection Module" and will henceforth be used throughout this paper, specifically in the legends of several figures. All experiments were performed with Type I ELMy H-mode plasmas.

The effect of local deuterium injection was investigated by replacing the standard divertor injection by OMP or top injection (or adding localized midplane gas in the case of DIII-D), with otherwise fixed plasma parameters. The coupling resistance R_c was evaluated using voltage and current probes in the transmission lines (AUG) or RF directional couplers (JET, DIII-D). Vacuum losses were accounted for. In these experiments, R_c was monitored as a function of the gas injection location, at different gas rates and different distances between the separatrix and the antenna. For the analysis, the measurements of R_c during ELMs were filtered-out since the inter-ELM phases correspond to the lowest coupling resistance and maximum antenna voltages. The electron density n_e was measured using mid-plane microwave reflectometers (AUG, JET, DIII-D), and Lithium beam diagnostics (AUG, JET). The effect of main chamber injection on other plasma parameters (impurity levels, confinement time, etc.) was also monitored.

It is worth reporting some implementation and operational limitations encountered during these experiments: on AUG, a poloidally distributed gas inlet integrated in an antenna limiter

Table 1: Tokamak and ICRF heating system parameters

	AUG	JET	DIII-D
ICRF system	four 2-strap antennas (1, 2, 3, 4) with: antennas 1 & 3 (boron coated limiters) and 2 & 4 (W coated limiters) paired by 3dB hybrid couplers.	four 4-strap antennas (A, B, C, D) with: - C and D paired by external conjugate T (ECT) junctions - A and B paired by 3dB hybrid couplers	three 4-strap antennas (called 285/300, 0, and 180 antennas)
f_{ICRF}	30 or 36.5 MHz	42 MHz	60 and 90 MHz
P_{ICRF} per antenna	10 kW to 0.8 MW	<1 MW	0.1 kW to 1 MW
Heating Scheme	N=1 (H)D minority	N=1 (H)D minority	ELD/TTMP
$k_{//,0}$ (m^{-1})	8 (π phasing)	6.6 (π phasing)	6 (285/300) & 7.4 (0,180) (π/2 phasing)
$n_{e,cut-off}$	5×10^{18} or 4×10^{18} m^{-3}	2×10^{18} m^{-3}	~1×10^{18} m^{-3}
$d_{strap-LCFS}$	9-14 cm	10-12 cm	10-16 cm
B_T/I_p	2T/0.8MA or 2.5T/0.8 MA	2.7T/2.5 MA	1.3-1.9 T / 1.3 MA
Plasma shape	Lower Single Null with cryo-pumped divertor		Double Null with cryo-pumped divertors
Other plasma heating	P_{NBI}=5MW P_{ECRH}=1.3 MW	P_{NBI}=13-15 MW	P_{NBI}=6-8 MW
Confinement regime	ELMy H-mode $H_{98(y,2)}\approx0.95$	ELMy H-mode $H_{98(y,2)}\approx0.8$	ELMy H-mode $H_{98(y,2)}\approx1$
Local gas flow	0.5-1×10^{22} el/sec	0.5-2×10^{22} el/sec	1.5×10^{22} el/sec

was also tested [9]. At the highest gas rates (~10^{22} el/s) however, the beneficial effect on antenna loading was hindered by an increased probability of arcing and a higher W sputtering yield at the limiter where the antenna valve was fitted. In this specific case, bringing the inlets outside the antenna box and retracting them radially could be an improvement. Gas fuelling must also be compatible with the operation of other systems and diagnostics; for example injecting gas too close from Li-beam diagnostics can compromise these measurements.

3. Experimental results

3.1. Effect of main chamber gas injection on ICRF antenna loading

On JET, AUG and DIII-D, midplane gas injection leads to a substantial increase of the coupling resistance of the antennas located close to the gas injection point. Examples for AUG and JET are shown in Figure 4. To normalize the differences in net fueling efficiency

of the different gas valves, R_c is plotted as a function of the sub-divertor pressure (AUG) or the intensity of the D_α emission in the outer divertor (JET). On both machines, and for all gas inlets, R_c increases when increasing the gas injection rate (and sub-divertor pressure), but in addition, antenna coupling resistance is maximized when using OMP gas injection close the active antenna(s).

In Figure 5, the coupling improvement (relative to the coupling obtained with divertor gas injection with similar rate) when using midplane injection or toroidally localized top injection is plotted as a function of the gas valve - antenna toroidal distance. For OMP injection this is defined as the toroidal distance in meters at the radial position of the antenna. For top injection, the gas injection – antenna distance is the shortest distance along the torus surface. For OMP injection, the coupling improvement decreases exponentially with the gas inlet-antenna distance with a characteristic decay length of ~ 2 meters on JET and ~ 4 meters in AUG (Figure 5) in these experimental conditions. Top gas injection leads to a (moderate) global improvement of the ICRF antennas loading, but no additional toroidally localized improvement is observed, even when the gas injection is magnetically connected to the antennas (see discussion in Section 3.3).

On all three devices, a SOL density increase is observed when using mid-plane or top gas (but with smaller effect) injection. An example for DIII-D is shown in Figure 6, where injecting ~2.6×10^{21} el/s close to the 285/300 antenna and to the 307 deg. reflectometer leads to an outward shift of 1 cm of the cut-off layer and an increase in the antenna coupling resistance [14]. The strong oscillations in the edge density are due to ELMs in these ELMy H-mode discharges. Other examples of SOL density measurements when using OMP injection are shown in Figure 7 (AUG) and Figure 8 (JET).

The antenna coupling resistance increase was found quantitatively consistent with the SOL density measurements in DIII-D [14], and JET [11] when the toroidal distance between the gas injection and the location of SOL measurements coincides with the gas injection-antenna distance. On JET, a simple 1D fast wave propagation and coupling code [11] with the plasma n_e profiles measured by the reflectometer (see Figure 2 for reflectometer position) was used to estimate the coupling resistance. The results are shown in Figure 9. A (unique) scaling factor was applied to the coupling resistance from the model to match the experimentally measured antenna-A coupling resistance when using divertor gas injection (module 11) with 1.8×10^{22} el/s. Highlighted in Figure 9 is the 50% increase in coupling resistance expected

from the density measurements (Figure 8) and the coupling model when changing the gas injection from divertor (module 11) to OMP (module 4), if an A2 antenna was located in front of the reflectometer line of sight. Taking into account the toroidal angle between the reflectometer and OMP gas injection location (module 4, which converts into 3 meters toroidal distance for R_{ant}=3.93 m), this expected antenna coupling increase is marked by a solid black square in Figure 5-b, and agrees well with the measured antenna coupling improvement when using OMP gas injection.

On AUG, two different approaches have be used to predict the expected coupling resistance increase from the measured density profiles when using OMP gas injection: (a) the same simple 1D antenna coupling model as just described together with reflectometry measurements; and (b) an extrapolation of the expected coupling improvement from the antenna "R_c experimental behavior" when moving the plasma outer radius. Both approaches gave the same result, the latter is described here: consistent with equation (2), the measured R_c during plasma outer radius scans using divertor gas injection can be fitted with an exponential of the form:

$$R_c \quad \propto \quad R_{c,0}\, e^{-\kappa\left(R_{ant}-R_{CutOff}\right)} \qquad (3),$$

where R_{ant} and R_{cutOff} are the radial position of the antenna and cut-off layer respectively; κ=18m^{-1} was fitted from the experimental data. From (3), the ~ 2cm shift in the cut-off density radial position observed by the reflectometry when using OMP gas from A03 (Figure 7) should lead to a 40 % increase of R_c if the antenna was located at the reflectometer toroidal position, ie 1.75 m away from the gas injection point. The same value of 40% increase in R_c is obtained from the simple 1 D coupling code using the measured density profiles. Both estimates are lower than the measured antenna R_c improvement during OMP gas injection (see Figure 5-a) even taking into account the experimental error bars. A possible explanation is that local modifications of the SOL density in front of the powered antenna (not captured by the currently available SOL measurements) are also occuring. In the next AUG campaign, the new 3 straps antenna [18] will be fitted with reflectometers which will allow measurement of the density directly in front of the antenna. This will hopefully shed some light on the possible density modifications driven by the ICRF power in front of the antennas: for example convective cells in front of the powered antennas [19], RF enhanced ionisation vs ICRF power induced density depletion as observed in both JET and AUG [20].

The effects of OMP gas injection on antenna loading is however reproduced for a large range of antenna power in different machines: few hundred watts to 1 MW in DIII-D, 10 kW to 1 MW range in AUG, and in the MW range in JET. Thus, if specific ICRF wave-SOL interaction effects can change the density in front of the powered antennas, the beneficial effect of local gas injection on antenna coupling appears to derive from the ionization of the neutrals by the plasma and subsequent local increase of the density in the SOL.

3.2. Effect of main chamber gas injection on plasma parameters

An important issue when considering gas injection from different locations is the consequence of using main chamber instead of divertor gas on plasma energy confinement: In JET and AUG, no degradation of confinement was observed when using the midplane or top inlets instead of the divertor inlets at the same gas fuelling level. An example for JET is shown in Figure 10 where for a data-base of H–mode pulses, the H factor $H_{98(y,2)}$ is plotted as a function of the D_α emission in the outer divertor (again to normalize for the differences in net fueling efficiency of the different gas valves). The quantity of gas required for antenna coupling improvement is also key, particularly since increasing gas dosing from the main chamber can have a negative impact on plasma energy confinement [21] in existing tokamaks. In this context it is important to emphasize that the antenna coupling improvements reported here are obtained when using moderate gas rates, and that this technique was used during the development of plasma scenarios in JET [22][24]. For example on AUG and JET, the improvement in the antenna loading was ~50% when fuelling the plasma only with nearby midplane inlets instead of divertor inlets at an injection rate compatible with the development of plasma scenarios: During the experiments described here, the normalised confinement enhancement factor was $H_{98(y,2)}\approx0.95$ with 0.75×10^{22} el/s injection rate in AUG [9], and $H_{98(y,2)}\approx0.8$ with 1.0×10^{22} el/s in JET. It is worth mentioning that the H-factor in these JET experiments is in line with the JET-ILW H-mode plasma database published in [23]. Understanding the modest confinement of JET-ILW plasma (compared to JET-C) is still the subject of active researches [24]. In these ICRF coupling experiments the strike point position being located away from the divertor pumping throat was also unfavourable. Better performance (for a given gas load) is obtained when putting the strike point closer to the pumping throat [24].

Optimized gas injection was found to be beneficial for reducing the W sputtering at the AUG antenna limiters [9][25]. On JET, a reduction of the plasma W [11] or Ni [26] content at mid-radius was also observed when using midplane or top inlets during ICRF heating. There are several possible explanations for these observations: (a) increased coupling resistance leads to a reduction of the RF fields which drives the RF sheath rectification responsible for the ICRF specific impurity release [27]; (b) a reduction of the SOL plasma temperature close to the gas injection which reduces the tungsten sputtering yield [28]; (c) the somewhat higher ELM frequencies observed on JET with main chamber gas injection can also contribute to the lower levels of impurities measured when switching from divertor to main chamber injection [29].

3.3. Effect of field line topology on SOL density during OMP and top gas injection

As an introduction to this section, it is useful to provide a simplified description of the mechanism leading to a local increase of the SOL density when using outer mid-plane (OMP) or top gas injection: the injected neutrals diffuse until they reach the plasma where they are ionized via electron impact. Neutral ionization is localized close to the entry point since the mean free path in a $n_e = 1\times10^{18}$ m^{-3} $T_e = 20$ eV plasma representative of the SOL conditions in AUG, DIII-D or JET is a few tens of centimeters. When using toroidally localized gas injection, as was the case for OMP and top gas injection in the experiments described in this paper, the SOL density is expected to be at least partially toroidally asymmetric. However, the competing processes of rapid plasma transport along magnetic field lines and cross-field particle transport in the SOL, coupled with the localized nature of the injection mean that the density build-up at the OMP where antennas are located is a strong function of magnetic field and injection geometry. These simple arguments can explain qualitatively what is observed regarding improvements in RF coupling resistance in the experiments reported here:

In the case of OMP injection close to an antenna, gas ionization occurs at short distance from the antenna (or directly in front of the antenna). For most of the magnetic field line configurations, the antenna is magnetically connected to the ionization source, or at short distance from field lines connecting to the ionization source; hence the electron density in front of the antenna is increased.

In the case of toroidally localized top gas injection, both on AUG and JET, a global and moderate increase of the SOL density and antenna coupling resistance was observed

experimentally, but the effect was spread evenly toroidally: R_c was slightly increased for all antennas around the torus. This can be qualitatively understood on the basis of magnetic field line geometry and is illustrated for JET and AUG in Figure 11 and Figure 12 respectively. Field line tracing in the magnetic equilibria used in the experiments shows how a density increase occurring on field lines at the top of the plasma would spread significantly in the toroidal direction at the midplane. In Figure 11 and Figure 12, the radial distance between the chosen field lines corresponds (+/- 0.5 cm) to the location of the cut-off at the plasma OMP in the respective experiments. In the JET case (Figure 11) the poloidal distance between the starting points of the field lines corresponds to the poloidal extent of the top gas injection. For AUG where top injection is from a single point (Figure 12), the poloidal range for the starting points is chosen to correspond with the extent of the SOL region with enhanced density when using top injection in the SOL modeling (see Section 4).

On JET, the poloidally distributed top gas injection is responsible for most of the toroidal spread encountered when the field lines run from top injection towards the OMP, as can be seen from the ~250 deg. toroidal difference at Z~0 between lines 1/4 and 2/3 (Figure 11).

In the AUG experiments, the higher upper triangularity leads to a secondary x-point at the top of the machine (see Figure 12) and the associated magnetic shear explains a large part of the toroidal spread encountered by field lines starting close to the top injection point (~200 deg. toroidal difference between line 2 and line 3 at Z~0 in Figure 12). The high field side position of the AUG top injection is also unfavorable to establish a localized connection along field lines to the OMP (distance between line 2 and line 3 compared to distance between line 1 and line 4 at midplane).

On ITER, main chamber gas injection will be from the top, low field side [15]. Injection piping will be routed through the upper port plugs and gas will be puffed into a space between the shield blocks and water cooling manifolds, from where it will diffuse out into the main chamber through the gaps (~20 mm wide) between blanket modules (BM). The entry location cannot be precisely controlled since gas diffuses in the interspaces, but it is expected to spread poloidally roughly over the extent of BM 11 and BM 12 (see Figure 12) and toroidally perhaps over the extent of a single BM (corresponding approximately to a toroidal angle of 10°). Figure 12 shows how the ITER ICRF antennas will be located in the OMP of port cells (PC) 13 and 15 and how field lines originating at different poloidal locations on BM11, 12 for gas injection from PC 10 will connect to the antennas for the baseline $Q_{DT} = 10$

equilibrium. On the basis of the results presented here, which show that some gain in coupling resistance is possible from localized top injection, ITER's gas injection system should allow some benefit for ICRF coupling. It will only be possible, however, to assess the potential gain through predictive simulations for ITER. This in turn can only be credible if results from today's experiments, reported here, can be satisfactorily modelled (see Section 4).

4. SOL modelling

Preliminary modelling of the JET [30] and AUG experiments has been performed using the EDGE2D-Eirene code package which couples the 2D plasma fluid code EDGE2D [31] with the kinetic neutral Monte-Carlo code Eirene [32]. No ICRF wave plasma interaction effects are included in these simulations. The simulations are performed in the usual way, adjusting transport parameters (notably $D_{\perp}$) to match SOL profiles, in the case here for discharges with gas puffing from the divertor. Switching the gas source position from divertor to OMP or top does show a density increase at the OMP but the magnitude of the SOL density increase cannot be quantitatively matched. For example on JET, the predicted shift in cut-off layer position (~2mm) is much smaller than experimentally observed via density measurements and from antenna coupling analysis (see Section 3.1). The main limitation of the current modelling is the 2D nature of the EDGE-2D code; in particular in the case of localized OMP injection, the neutral pressure and ionization source close to the injection point is underestimated (assumed uniform in the toroidal direction in the simulation).

A more realistic simulation must include 3D effects and this has started for AUG [33] using the EMC3-Eirene code package, where EMC3 is a 3D Monte Carlo plasma fluid code [34]. A comprehensive description of these EMC3 simulations for the AUG experiment will be reported in a separate paper. The AUG geometry is fully described in the code, in particular the toroidally non-axisymmetric nature of the plasma facing components, and the location of the gas valves. Again, no ICRF wave plasma interaction effects are included in these simulations. As in the EDGE2D-Eirene approach, the transport coefficients are first adjusted to provide a best match to measured upstream (SOL density measured by the Li-beam diagnostic) and divertor plasma parameters (divertor probes saturation current) for the case of toroidally distributed divertor injection. Injection is then switched in the simulations to a toroidally localized OMP or top source. In common with experiment, top injection leads

to an increase in the SOL density at the OMP (~ 5mm shift of the cut-off), but it is not toroidally localized; this is a consequence of the toroidal spreading of the field lines in this magnetic configuration as explained in Section 3.3. OMP gas injection leads to a larger density increase in the midplane and it is toroidally localized close to the gas injection location, in line with the experimental findings. An example of an EMC3 simulation with OMP injection is shown in Figure 14. The EMC3 density profiles are plotted at the reflectometer location using 1.2×10^{22} el/sec gas from divertor or the OMP A03 valve located ~45 deg toroidally from the reflectometer. In the simulations, the cut-off density at the reflectometer is shifted by ~ 2 cm when using A03 OMP gas puff which is in agreement with the measurements in similar conditions (see Figure 7), giving confidence that EMC3 can accurately describe the effect of local gas puffing on the SOL in AUG. A more detailed analysis where the EMC3 SOL profiles are used in the FELICE [36] wave propagation and coupling code to calculate the expected antenna coupling resistance is reported in [35].

5. Conclusions and Prospects

The experiments coordinated by the ITPA in AUG, JET and DIII-D have demonstrated that OMP gas injection strongly enhances the coupling resistance of nearby ICRF antennas. The effect is substantial at moderate gas rates (~10^{22} el/sec) which are compatible with the development of high performance scenarios. On JET and DIII-D, the measured SOL density increase when using main chamber puffing is consistent with the antenna coupling resistance increase provided that the distance between the measurement Line of Sight and the injection location is taken into account. On AUG, the measured antenna coupling resistance improvement is larger than expected from SOL measurements, suggesting that local SOL modifications in front of the antennas may also play a role. Top gas injection leads to a global density increase in the OMP with a smaller and uniform (for all the antennas around the torus) increase in the antenna coupling resistance. This latter result is explained in terms of the specific plasma configuration in the experiments (secondary x-point in AUG) and the geometry of the gas inlets (top gas injection poloidally distributed in JET).

In this respect the planned ITER gas injection system is favorable, but more simulation work is needed to quantitatively assess the capability of top low field side injection to increase the density in front of the ITER ICRF antennas. These simulations must involve 3D SOL codes (benchmarked against present experiments) to properly describe the toroidally localized

ionization sources and the magnetic field line topology. Interpretation of AUG results using EMC3-Eirene is being performed and the strong localized effect of OMP injection can be reproduced. Benchmarking of the code against today's experiments must be performed before any application to ITER can be made with confidence.

Acknowledgements

The views and opinions expressed herein do not necessarily reflect those of the ITER Organization or of the European Commission. This work has been carried out within the framework of the EUROfusion Consortium and has received funding from the Euratom research and training programme 2014-2018 under grant agreement No 633053. The views and opinions expressed herein do not necessarily reflect those of the European Commission. This work was also part-funded by the RCUK Energy Programme under grant EP/I501045.

References

[1] STIX, T., 1992 "Waves in Plasmas", AIP Press, ISBN 0-88318-859-7.

[2] Bilato R., Brambilla M., Hartmann D.A. and Parisot A. 2005 Nucl. Fusion 45 L5–7

[3] Bobkov V. et al 2006 Nucl. Fusion 46 S469–75

[4] F. Clairet, L. Colas, S. Heuraux and G. Lombard Plasma Phys. Control. Fusion 46 (2004) 1567–1580

[5] A. Messiaen, et al., Nucl. Fusion 50 (2010) 025026

[6] F. Durodié, et al., Physics of Plasmas 21, 061512 (2014)

[7] M-L. Mayoral, et al., Proc. 23rd IAEA FEC (2010), P1-11

[8] A. Ekedahl, et al., Plasma Phys. Control. Fusion 54 (2012) 074004 (7pp)

[9] V. Bobkov, et al., AIP Conf. Proc. 1580, 271 (2014)

[10] P. Jacquet, et al., Nuclear Fusion 52 (2012) 042002

[11] E. Lerche, et al, Journal of Nuclear Materials 463 (2015) 634–639 , http://dx.doi.org/10.1016/j.jnucmat.2014.10.074

[12] M.-L. Mayoral et al., AIP Conf Proc. 933 (2007) p.55

[13] Pinsker R.I., et al., 37th EPS Conf. (2010) http://ocs.ciemat.es/EPS2010PAP/pdf/O4.124.pdf

[14] Pinsker R.I., et al., AIP Conf Proc. 1406 (2011) p.313

[15] S. Maruyama, et al., Proc. 23rd IAEA FEC (2010), P5-24

[16] S. Maruyama, et al., Proc. 24st IAEA FEC (2012), P1-28

[17] Peter C Stangeby, "The Plasma Boundary of Magnetic Fusion Devices", Institute of Physics Publishing (2000), ISBN 0 7503 0559 2.

[18] V. Bobkov et al., Nucl. Fusion 53 (2013), 093018

[19] Becoulet M. et al 2002 Phys. Plasmas 9 2619–32

[20] L. Colas, et al, Journal of Nuclear Materials 463 (2015) 735–738, http://dx.doi.org/10.1016/j.jnucmat.2014.10.011

[21] G. Saibene, et al, Nucl. Fusion 39 (1999) 1133–56

[22] C. Giroud, et al., " Towards Baseline Operation Integrating ITER-Relevant Core and Edge Plasma within the Constraint of the ITER-likeWall at JET" Proceedings of the 25th IAEA Fusion Energy Conference 2014, Saint Petersburg, Russia, EX/P5-25

[23] M.N.A Beurskens, et al., Nucl. Fusion 54 (2014) 043001

[24] I. Nunes, et al., " Compatibility of high performance operation with JET ILW" Proceedings of the 25th IAEA Fusion Energy Conference 2014, Saint Petersburg, Russia, EX/9-2

[25] V. Bobkov, et al., Nucl. Fusion 53 (2013) 093018

[26] A. Czarnecka, et al., Plasma Phys. Control. Fusion 54 (2012) 074013

[27] Perkins F.W. et al 1989 Nucl. Fusion 29 583–92

[28] V. Bobkov, et al., Nucl. Fusion 50 (2010) 035004

[29] R. Dux, et al., Journal of Nuclear Materials 390–391 (2009) 858–863

[30] V. Petrzilka, et al., 39th EPS Conference on Plasma Physics (2012), P2.027

[31] R. Simonini et al., Contribution to Plasma Physics 34 (1994) 368

[32] S. Wiesen, www.eirene.de/e2deir_report_30jun06.pdf

[33] W. Zhang, et al., "Simulations of gas puff effects on edge density and ICRF coupling in ASDEX Upgrade using EMC3-Eirene", accepted contribution 21st Topical Conference on RF Power in Plasmas, 27-29 April 2015, Lake Arrowhead, California, USA.

[34] Feng Y. et al. Contrib. Plasma Phys. 44 (2004) No. 1–3, 57–69

[35] V. Bobkov, et al., "Progress in controlling ICRF-edge interactions in ASDEX Upgrade", accepted contribution 21st Topical Conference on RF Power in Plasmas, 27-29 April 2015, Lake Arrowhead, California, USA.

[36] M. Brambilla, Nuclear Fusion 35 (1995), 1265-1280.

Figures

Figure 1. Top view (a) and poloidal cross-section (b) of AUG illustrating the position of the ICRF antennas and the location of the gas inlets. The SOL diagnostics lines of sight are also indicated.

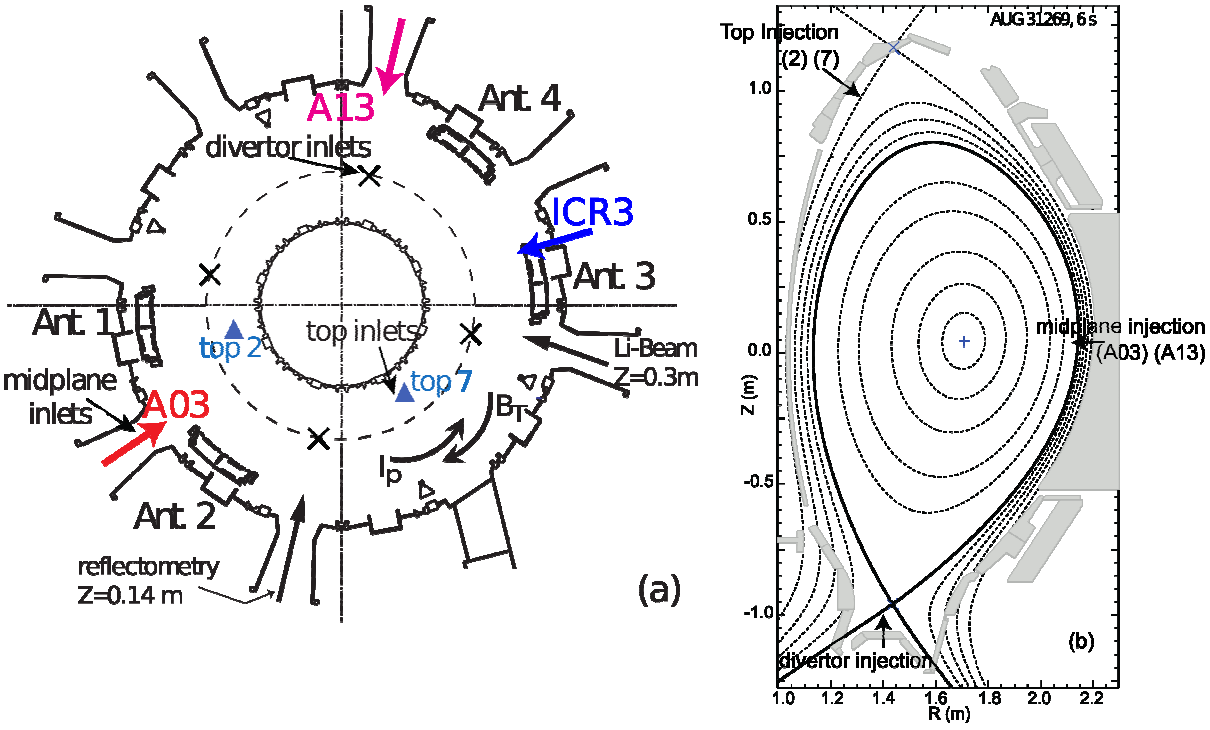

Figure 2. Top view (a) and poloidal cross-section (b) of JET illustrating the position of the ICRF antennas and the location of the gas inlets. At each toroidal location (GIM7 or GIM8) the top gas injection is poloidally distributed. The SOL diagnostics lines of sight are also indicated.

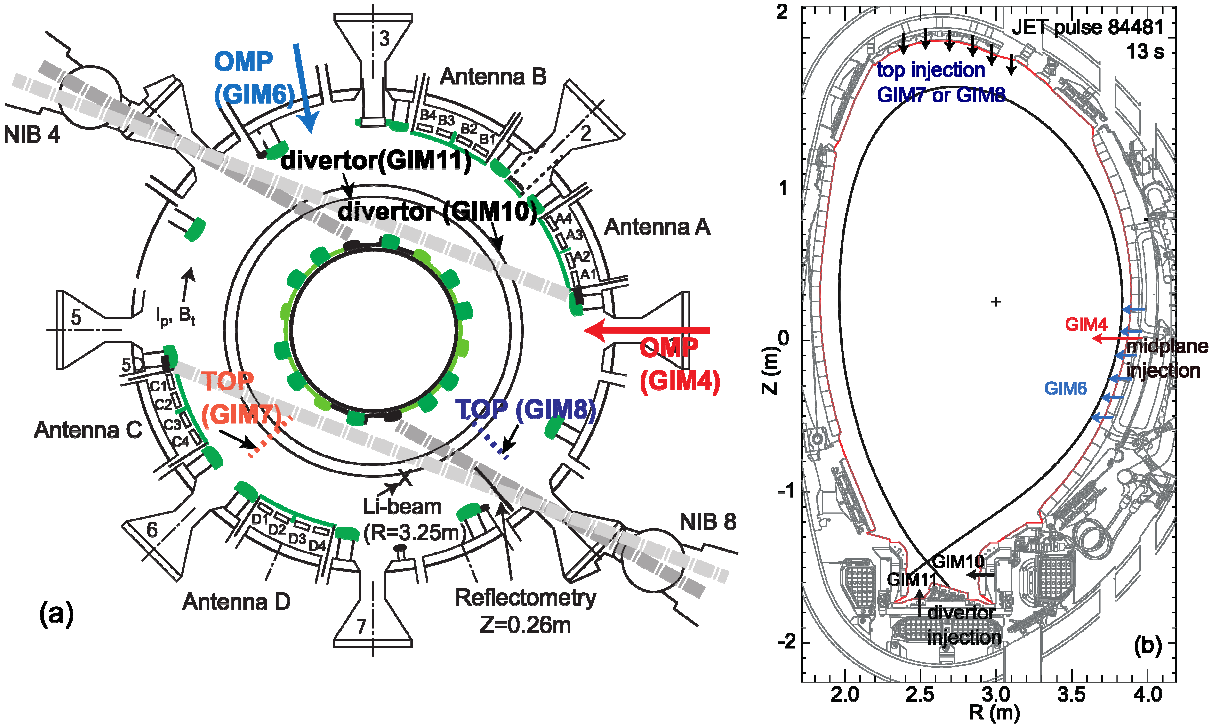

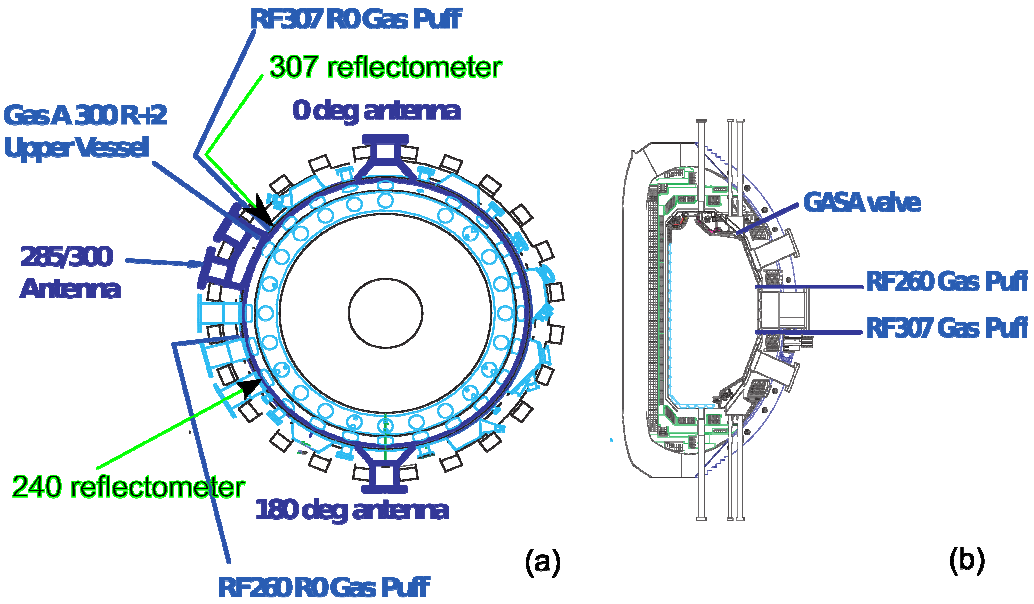

Figure 3. Top view (a) and poloidal cross-section (b) of DIII-D illustrating the position of the ICRF antennas and the location of the gas inlets. The SOL diagnostics lines of sight are also indicated.

Figure 4. Antenna coupling resistance using divertor, outer mid-plane or top gas inlets (see Figure 1 for exact locations). (a) AUG Antenna 1, Rc is plotted vs the sub-divertor pressure, injection rate is in the range 0.5-1.3×10^{22} el.s^{-1}; $d_{Antenna-LCFS}$=5 cm. (b) JET antenna , Rc is plotted vs the D_α emission intensity in the outer divertor, injection rate is in the range 0.5-1.7×10^{22} el.s^{-1}; $d_{Antenna-LCFS}$=5.5 cm.

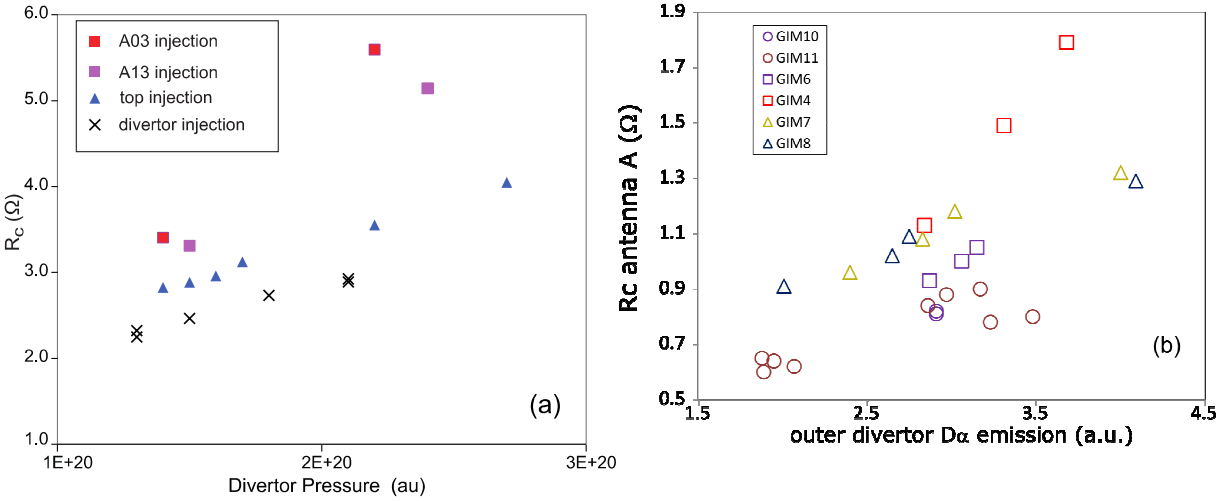

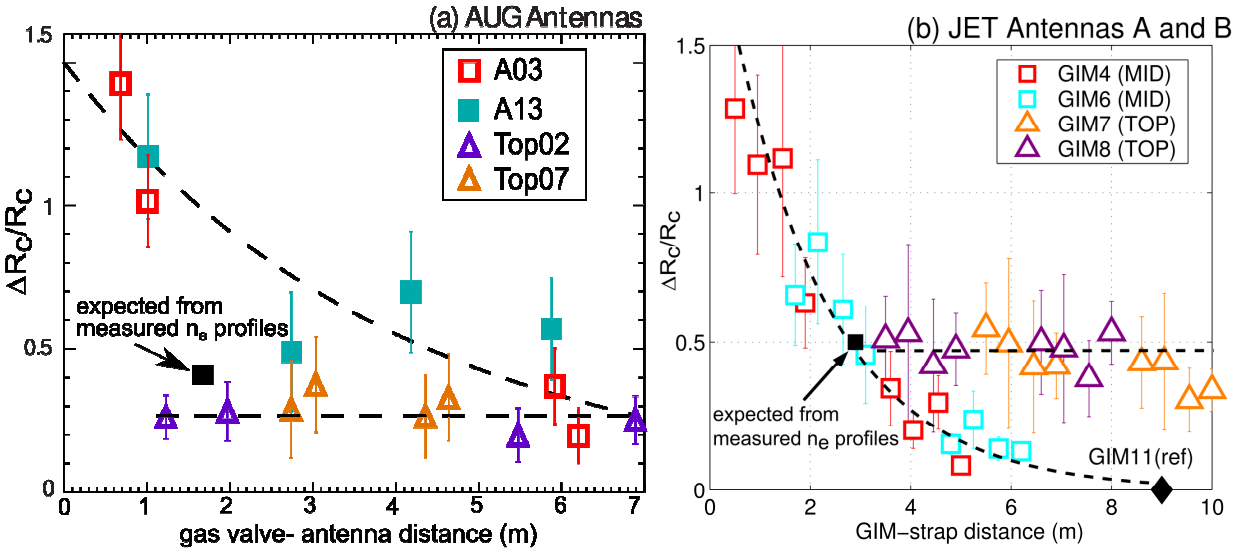

Figure 5. ***AUG (a) and JET (b), relative coupling resistance increase of the antenna straps w.r.t divertor fuelled discharges plotted as a function of the injection-antenna distance. For AUG, the data-set includes the 4 antennas using A03, A13, Top2 and Top7 injection (see*** **Figure 1-*a)*** ***at rate ~1.2×10^{22} el.s^{-1}. For JET, GIM 4, 6, 7 and 8 (see*** **Figure 1-*b)*** ***at rate [1.6-1.8]×10^{22} e/s were used. In (b), the black solid square is the coupling improvement expected from the simple 1D code using density profiles from reflectometry (see also Figure 9). In this case, the toroidal distance between the reflectometer Line-of sight and the gas inlet (GIM4) is the abscissa.***

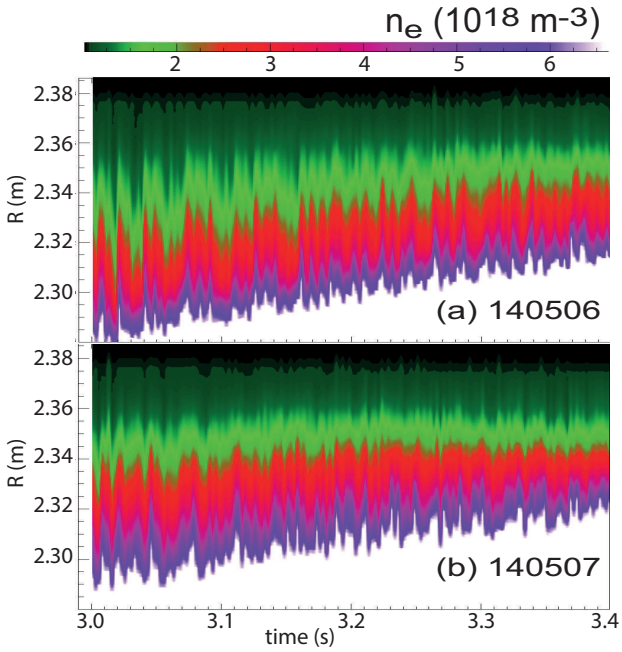

Figure 6. ***On DIII-D, density profiles measured at port 307deg, without (a) or with (b) 2.6×10^{21} el/s injection from a local midplane valve (FW307 in*** **Figure 1-*c*).** ***In both discharges, the outer gap was ramped from 8 cm (3s) to 3 cm (3.4s) and the power applied to the 285/300 antenna was 0.1kW.***

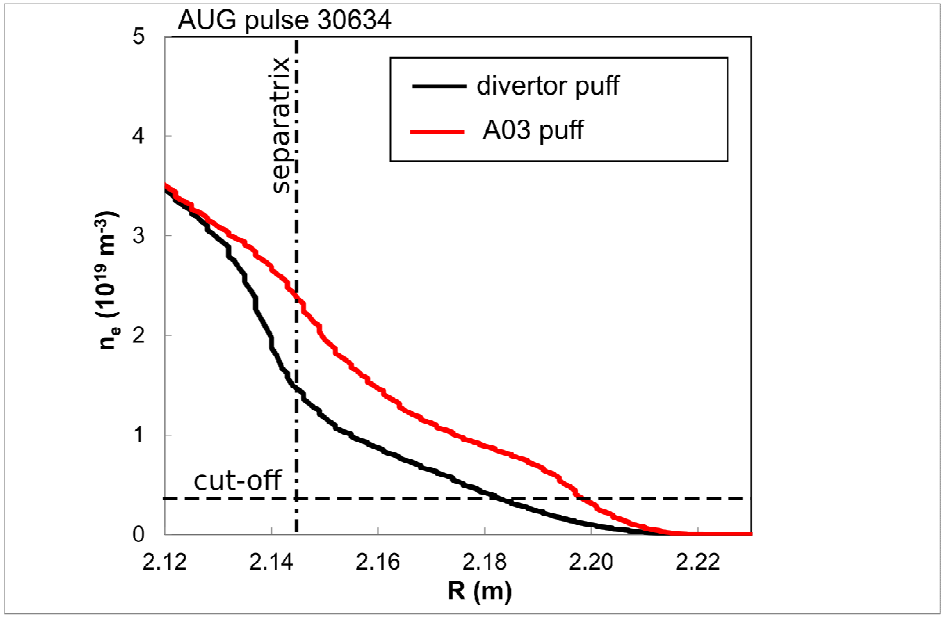

Figure 7. For AUG, SOL density measured by the reflectometer in sector 5 when using divertor (black) or sector 3 (A03) OMP gas puff (red). The profiles are averaged over a 0.2 s period at 2.2 sec (divertor injection) and 6.0 sec (A03 OMP injection). Profiles during ELM events were filtered out.

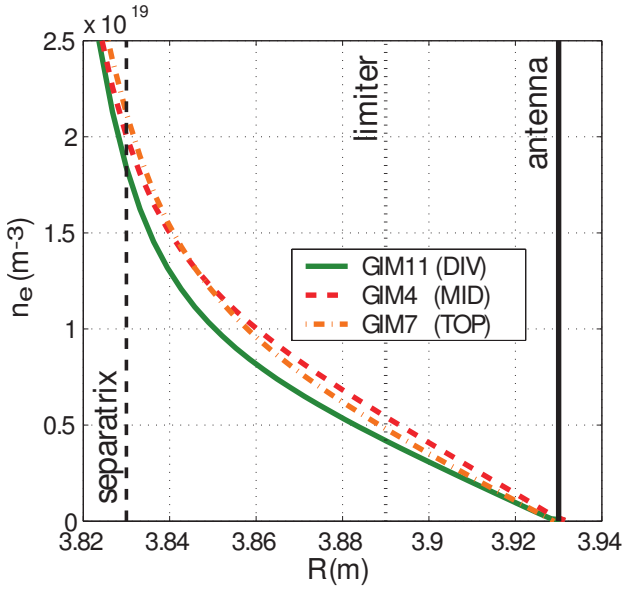

Figure 8. ***On JET, density profiles measured by reflectometry. Data are averaged over 1 s and ELMs are filtered out. The flow rates are GIM11:1.85×10^{22}el/sec; GIM4:1.65×10^{22}el/sec; GIM7:1.6×10^{22}el/sec.***

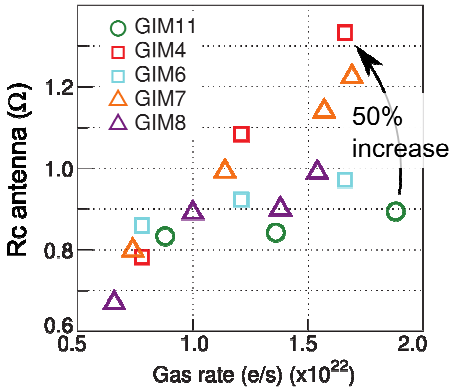

Figure 9. For JET, antenna coupling resistance calculated using a simple 1D coupling code with the density profiles from reflectometry as input. The points used to calculate the 'expected' coupling improvement at the reflectometry line of sight and reported in Figure 5-b are indicated with arrows.

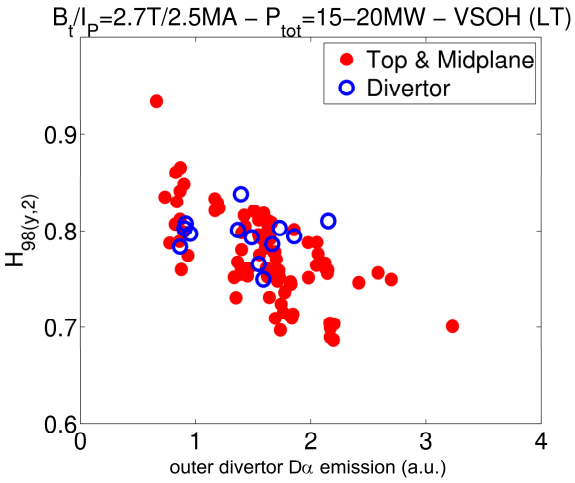

Figure 10. ***JET, $H_{98(y,2)}$ vs outer divertor D_α emission for a series of pulses with divertor or (midplane+top) gas injection. Injection rate is in the range 0.5×10^{22}-2.7×10^{22} el/s. This data-set fits in the JET-ILW confinement data-base (low triangularity baseline scenario) described in [23].***

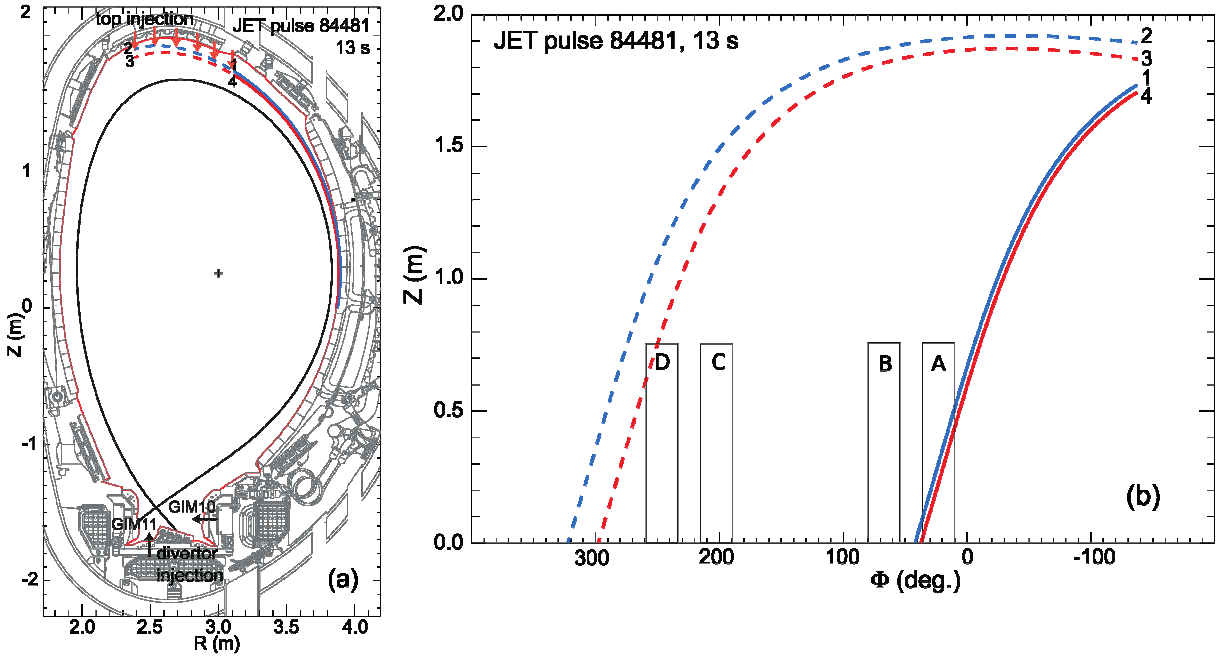

Figure 11. For JET, ***(a) poloidal cross sections showing the location of gas injection at one top toroidal location (GIM7) and field lines starting from the top of the plasma; (b) Field lines in the (Φ,Z) plane (looking from the plasma). Field lines (starting points 1, 2, 3, 4) are mapped to R=3.885m and R=3.895m at the plasma midplane (cut-off location +/- 0.5 cm).***

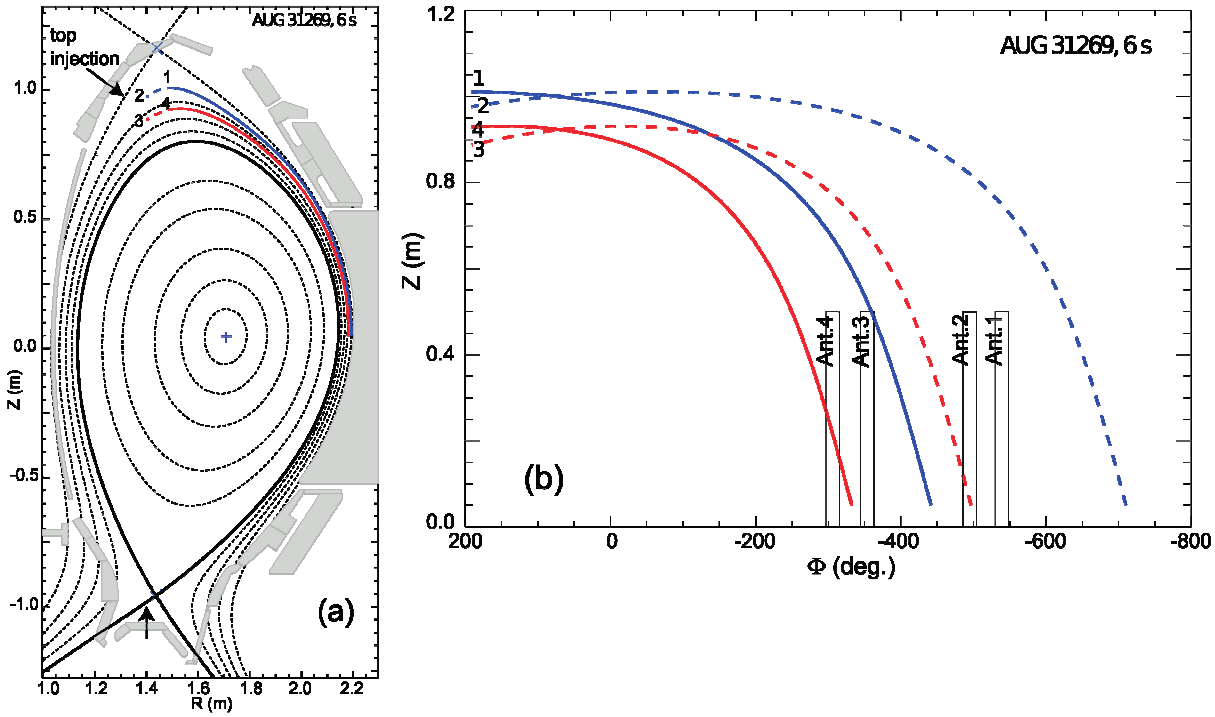

Figure 12. For AUG, ***(a) poloidal cross sections showing the location of gas injection at one top toroidal location (Top2) and field lines starting from the top of the plasma; (b) Field lines in the (Φ,Z) plane (looking from the plasma). Field lines (starting points 1, 2, 3, 4) are mapped to R=2.18m and R=2.19m at the plasma midplane (cut-off location +/- 0.5 cm).***

–

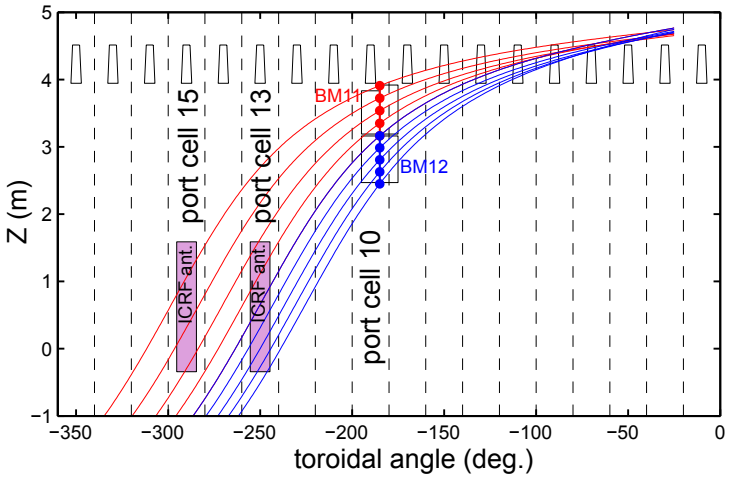

Figure 13. For ITER, example of field lines starting next to the Blanket modules 11 (red) and 12 (blue) in port cell 10. Plasma parameters are for the Q_{DT}=10 15 MA reference scenario.

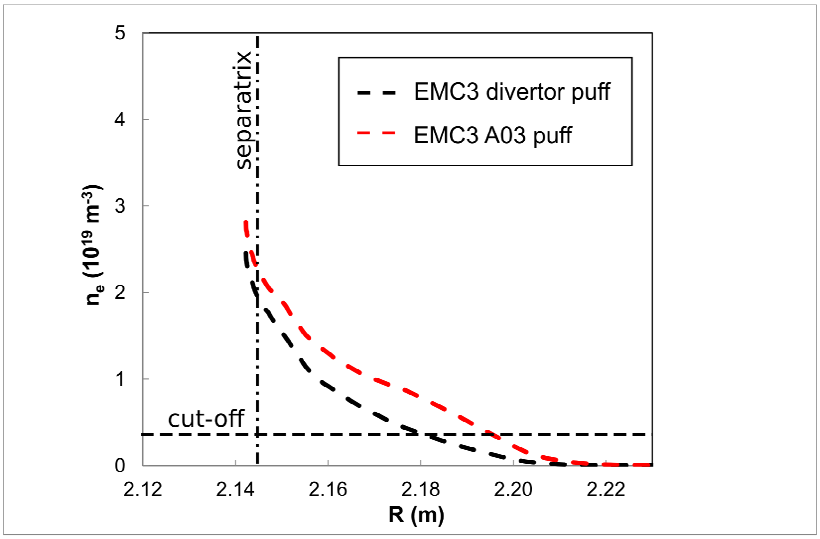

Figure 14. AUG SOL profiles from EMC3-EIRENE simulations at the reflectometer line of sight when using divertor or OMP A03 gas injection. EMC3 simulations parameters were adjusted to fit Li-beam and divertor plasma measurements for pulse 31269 with divertor gas injection.